Food Research International 197 (2024) 115125

Contents lists available at ScienceDirect

Food Research International

journal homepage: www.elsevier.com/locate/foodres

A study of the oral bioavailability and biodistribution increase of Nanoencapsulation-driven Delivering radiolabeled anthocyanins

Thiécla Katiane Osvaldt Rosales [a,b,i], Fábio Fernando Alves da Silva [b], Andy Gonzàlez Rivera [c], Sofia Nascimento dos Santos [d], Daniel Bustos [e], Luis Alberto Morales-Quintana [f], Hélder A. Santos [g,h], Emerson Soares Bernardes [b], João Paulo Fabi [a,i,j,*]

[a] Department of Food Science and Experimental Nutrition, School of Pharmaceutical Science, University of São Paulo, São Paulo, SP, Brazil
[b] Instituto de Pesquisa Energéticas e Nucleares – IPEN, São Paulo, SP, Brazil
[c] Molecular Imaging Research Program, Division of Nuclear Medicine, Department of Radiology, Mayo Clinic, Rochester, MN, USA
[d] Department of Imaging Chemistry and Biology, King's College London - London, United Kingdom
[e] Laboratorio de Bioinformática y Química Computacional, Departamento de Medicina Traslacional, Facultad de Medicina, Universidad Católica del Maule, Talca 3480094, Chile
[f] Multidisciplinary Agroindustry Research Laboratory, Instituto de Ciencias Biomédicas, Facultad de Ciencias de la Salud, Universidad Autónoma de Chile, Cinco Poniente #1670 Talca, Región del Maule, Chile
[g] Department of Biomaterials and Biomedical Technology, The Personalized Medicine Research Institute (PRECISION), University Medical Center Groningen, University of Groningen, Groningen, the Netherlands
[h] Drug Research Program, Division of Pharmaceutical Chemistry and Technology, Faculty of Pharmacy, University of Helsinki, Helsinki, Finland
[i] Food Research Center (FoRC), São Paulo, SP, Brazil
[j] Food and Nutrition Research Center (NAPAN), University of São Paulo, São Paulo, SP, Brazil

ARTICLE INFO

Keywords:
Absorption
Cyanidin-3-*O*-glucoside
Molecular Image
Nanoencapsulation
Pectin
Lysozyme

ABSTRACT

Anthocyanins have antioxidant, anti-inflammatory, and anticancer properties but have limited bioaccessibility and bioavailability due to molecular instability in the gastrointestinal tract. This study evaluated the absorption and biodistribution of free and nanoencapsulated radiolabeled anthocyanin (cyanidin-3-*O*-glucoside). A new methodology was efficiently developed for radiolabeling anthocyanins with Technetium (^{99m}Tc-anthocyanins). Then, the anthocyanins were nanoencapsulated through self-assembly using citrus pectin and lysozyme. The nanostructures have a size of 190 nm, a zeta potential of –30 mV, and an invariably spherical and homogeneous morphology. The biodistribution in different tissues, the kinetics of absorption, and molecular visualization by micro single-photon emission computed tomography/computed tomography (μSPECT/CT) showed that the nanoencapsulated anthocyanins are absorbed differently than free anthocyanin in mice. After oral administration, nanostructured anthocyanins were delivered to the blood, spleen, bladder, pancreas, and bone, unlike unencapsulated anthocyanins found only in kidneys and bladder. *In silico* data indicated the stabilization between compounds in nanocapsules and demonstrated the pH-dependent release of anthocyanins in the intestine. The nanoencapsulation alters the absorption kinetics, increasing the blood's bioavailability and the organs' uptake, suggesting an improvement of the biological effects and potential clinical application.

1. Introduction

Anthocyanins, a subclass of flavonoids, are water-soluble compounds that occur naturally in colorful plants (Igwe et al., 2019), such as blue, red, and purple-colored ones, for example, blackberries, blueberries, grapes, and strawberries (Qi et al., 2023). Anthocyanins are the glycosylated forms of anthocyanidins (aglycones) and are structurally composed of a flavylium cation backbone hydroxylated in different positions (Manolescu et al., 2019; Custodio-Mendoza et al., 2024). They have multiple biological activities, such as antioxidant, anti-inflammatory, and anticancer (Bondonno et al., 2019; Tena et al., 2020).

These bioactive compounds are promising for reducing the risk of developing chronic diseases and are effective for neurological, endocrine, immunological, skeletal, and cardiovascular disorders. Hence,

* Corresponding author.
E-mail address: jpfabi@usp.br (J.P. Fabi).

https://doi.org/10.1016/j.foodres.2024.115125
Received 30 July 2024; Received in revised form 19 September 2024; Accepted 20 September 2024
Available online 24 September 2024

anthocyanins are potential molecules for adjuvant treatment and as an alternative for personalized therapies (Kapoor et al., 2023; Xue et al., 2023).

However, the molecular instability of these compounds leads to low absorption, limited reach to specific tissues, and restricted biological use (Braga et al., 2018). Factors associated with human digestion, such as pH, enzyme action, and intestinal bacteria, are responsible for intense degradation in the gastrointestinal tract (Victoria-Campos et al., 2022). Moreover, nanoencapsulation is considered viable for maintaining the molecular integrity of anthocyanins (Rosales et al., 2023a). The development of nanostructures based on citrus pectin and lysozyme by molecular self-assembling demonstrated that anthocyanins could be physically and chemically stabilized under physiological conditions (Osvaldt Rosales et al., 2021), accurately released in the intestinal phase in a system simulating digestion, and recognized by cells *in vitro* (Brodkorb et al., 2019; Rosales et al., 2023b). These results suggest that following oral ingestion, the pectic nanostructures can protect anthocyanins from intrinsic digestion factors and can promote effective absorption of (1) anthocyanin molecules released in the intestine and absorbed by passive or active diffusion by enterocytes and (2) nanocapsules can be fully absorbed and release into the cell interior, circulation, and target specific tissues (Salarbashi et al., 2020).

Comprehending the processes involved in the biodistribution of nanoencapsulated anthocyanins orally administered is essential to establishing targeted therapies at specific sites in the body (Jaime & Santoyo, 2021). Therefore, the precise quantification of delivery to each tissue and molecular imaging assessment of the distribution of these nanoencapsulated compounds constitute tools for understanding the absorption, metabolism, and excretion after oral ingestion, which have not yet been elucidated in the literature (Hee et al., 2016). Moreover, determining the biological pathway of nanoencapsulated anthocyanins is essential for developing new dietary supplements for precisely targeted delivery systems.

In this study, we analyzed the biodistribution of radiolabeled and nanoencapsulated anthocyanin in an animal model to understand the biological destination compared to the free molecule (unencapsulated). A new methodology was developed to radiolabel with Technetium (^{99m}Tc), the anthocyanins extracted and isolated from blackberry (*Rubus* spp.). In addition, *in silico* tools were used to understand the probable bounds between the radioisotope and the anthocyanins complexes. We applied a nanoencapsulation method based on citrus pectin and lysozyme and evaluated the biodistribution, kinetics of absorption, and molecular visualization by μSPECT/CT in mice. Moreover, the *in silico* interaction of anthocyanins with the encapsulating biomaterial was conducted to understand the gastrointestinal tract's pH-dependent release process and the impact on retention time and absorption. Our results provide further knowledge about the bioavailability of nanoencapsulated anthocyanins, thus prospecting the technology for future clinical applications.

2. Material and methods

2.1. Solvents, reagents, and general experimentation procedures

The blackberries (*Rubus* spp.) were commercially obtained (Berry Good®) at the ripe stage and were suitable for consumption. They were cleaned and sanitized (Sodium Hypochlorite at 100 ppm). Commercial citrus pectin (#P9135), with a degree of esterification of 64 % (Silva et al., 2022), lysozyme (*N*-acetylmuramide glycohydrolase) (#12650–88-3), and other reagents used for general experimentation procedures were purchased from Sigma-Aldrich®.

2.2. Obtaining and enriching anthocyanin extract from blackberry

Anthocyanins were extracted from blackberries (*Rubus* spp.); five grams of fresh fruit were pulverized in liquid nitrogen and homogenized in an Ultraturrax (Polytron Kinematica GnbH, Kriens-Luzern, Switzerland) with 70 % methanol in water and 0.2 % Acetic Acid (Teixeira et al., 2015). Afterward, the extract was filtered under a vacuum and rotary evaporated (T<40°C) to remove methanol. For enrichment, the extract was filtered through a polyamide-CC-6 column (MACH-104 8156201) (Macherey-Nagel, Bethlehem, PA, USA), eluted with 70 % acidified methanol (0.2 % HCl), and rotary evaporation (T<40°C) (Osvaldt Rosales et al., 2021). Finally, the extract was dissolved in methanol (5 % HCl) for HPLC-DAD or milli-Q water for nanostructures formulation.

2.3. Identification and quantification of anthocyanin

For the identification and quantification of anthocyanin, the enriched extract was filtered through a 0.22 μm PTFE membrane (Millipore Ltd., Bedford MA) and analyzed with the Infinity Quaternary LC system (Agilent Technologies, USA), with autosampler (chamber set to 4 °C protected from light) and a quaternary pump, coupled to a diode array detector (DAD). The column was Agilent Zorbax Eclipse Plus C18 (5 μm, 4.6 × 250 mm). The elution solvents were solvent A, 0.10 % trifluoroacetic acid in the water, and solvent B, 0.10 % methanol acid in acetonitrile. The solvent gradient was applied as follows: 100 % A at the beginning, 100 % B at 10 min, 100 % A at 15 min, and 100 % B at 20 min. The chromatograms were fully scanned from 220 – 700 nm (flow rate of 1 mL/min and a column temperature of 25 °C). Anthocyanins were identified by comparing the retention time (RT) and diode array spectral characteristics with commercial standard and literature data. They were quantified using a calibration curve of cyanidin-3-*O*-glucoside (C3G) standard (Extrasynthese, Genay, France) acquired at 525 nm (Teixeira et al., 2015).

Chromatographic analyses were used to compare the RT of a free radioactive compound (Technetium) and radiolabeled anthocyanin (^{99m}Tc-anthocyanin) using the same methodology described above but with a radiometric detector. The radiolabeled complex (^{99m}Tc-anthocyanin) was injected with an activity of 1.85 MBq, and the results demonstrate the interaction between ^{99m}Tc and C3G.

2.4. Radiolabeled anthocyanins: Development of a new methodology

2.4.1. Chemicals, radiolabeling, and quality process

Anthocyanin extract (0.75 mg/mL) was diluted in water MiliQ, and a 150 μL of anthocyanin extract aliquot was used for the reaction (protect from the light). The direct radiolabeled was realized with a mix of 150 μL and 20 μg $SnCl_2$ (4 mg/mL in 0.01 N HCl previously in gaseous nitrogen solution for 10 min) and nitrogenized for 5 min. Afterward, ^{99m}Tc (pertechnetate eluted from ^{99}Mo column) (185 MBq) (obtained from Instituto de Pesquisas Energéticas e Nucleares – IPEN, São Paulo, Brazil) was added, and the mixture was nitrogenized for 10 min and incubated for 40 min. The $SnCl_2$, ^{99m}Tc, anthocyanin concentration, and pH were optimized for the maximum labeling efficiency (≥95 %). The ^{99m}Tc–anthocyanin (0.5 MBq) quality control assay was performed by Instant Thin Layer Chromatography – ITLC-SG (Agilent Technologies, CA, USA) ascending paper with two different mobile phases: 1) 100 % methyl ethyl acetone, and 2) pyridine: ethanol: water (1:2:5). In the first phase ^{99m}Tc – anthocyanin and the reduced hydrolyzed technetium species (R/H ^{99m}Tc) – remained at the point of application (Rf = 0) and ^{99m}Tc free run (Rf = 1). In phase two, ^{99m}Tc-anthocyanin was run with the mobile phase (Rf = 1) and remained in stationary phase R/H ^{99m}Tc and ^{99m}Tc free (Rf = 0). The percentage proportions of every species were quantified, and the radiochemical purity was measured using a Wizard 2 2480 automatic gamma counter. Quality control analysis resulted in more than 95 % radiochemical purity.

2.4.2. Characterization and in vitro stability of radiolabeled ^{99m}Tc-anthocyanin

The stability of ^{99m}Tc – anthocyanin was carried out in saline and

mice blood plasma. For this, 10 μL (10 MBq) of ^{99m}Tc – Anthocyanin was added to 100 μL of saline solution (0.9 % NaCl), and in 100 μL of blood plasma from Balb/C mice, extracted by cardiac puncture, heparinized (60 U/mL at 10 %) and centrifuged at 12,000 RPM (5 min). The analyzed times were 0, 0.5, 1, 2, 3, 4, 5, 6, and 24 h. Quality control was performed using ITLC-SG (Agilent Technologies, CA, USA), as described in item 2.4.1.

2.5. In silico modeling of radiolabeled anthocyanin

The chemical structures were initially drafted using ChemDraw (version 22.2.0) and pre-optimized in Chem3D (version 22.2.0) using the molecular mechanic's method (MM2). Subsequently, complete geometry optimization of the complexes was conducted employing the DFT method through the ORCA program (version 5.0). In this process, the functional B3LYP was applied alongside the STO-3G basis set for atoms with Z<16, while the LanL2DZ basis set was used for the ^{99m}Tc.

2.6. Development and characterization of pectin/lysozyme ^{99m}Tc-anthocyanin-loaded nanostructure

The nanostructures were prepared according to Osvaldt Rosales et al., 2021, the pectin solution with an initial pH of 5 was adjusted to pH 10 by adding 0.1 M NaOH (1 mg/mL). Lysozyme solution (2 mg/mL at pH 9) and ^{99m}Tc – anthocyanin solution (0.75 mg/mL at pH 3) were monitored for constant pH maintenance. The ^{99m}Tc-anthocyanin solution was combined with a ratio of 1:2:0.4 (m:m:m) (pectin, lysozyme, and ^{99m}Tc-anthocyanin, respectively). The pectin and lysozyme solutions were heated separately at 80 °C for 30 min, after being subjected to rapid cooling until reaching a temperature of 4 °C (30 min on ice). The anthocyanin solution was maintained at 4 °C (protect from the light). The mixture occurred with final concentrations: pectin (0.3 mg/mL), lysozyme (0.6 mg/mL), and ^{99m}Tc-anthocyanin (0.1 mg/mL), and with constant pH control (final pH 5) and magnetic agitation (300 rpm for one hour). Afterward, the nanostructures were centrifuged through an Amicon filter (10 kDa MWCO Amicon filter) (30 min, RCF 289 g). The retained nanoparticles were used for the downstream methodologies, and the filtrate was analyzed to quantify the efficiency of the encapsulation process. All methods were conducted after 10 half-lives of ^{99m}Tc (60hs), where no radiation was detected, despite the *in vivo* tests where nanoparticles were administered to mice right after synthesis.

2.6.1. Encapsulation efficiency (%)

Unencapsulated anthocyanins were quantified by spectrophotometric analysis at different pH levels. The anthocyanin concentration was calculated using the molar extinction coefficient of the C3G (ϵ = 26900) and λ_{ex} 520 nm and λ_{em} 700 nm, and distilled water as a blank (Giusti & Wrolstad, 2005). The results were expressed as the milligram equivalent of C3G, according to Eq. (1):

$$\text{Anthocyanin}(\text{mg/L}) = \frac{A \times MM \times Fd}{\varepsilon \times 1} \times 1000 \quad (1)$$

wherein: A = (Abs510 nm − Abs700nm) pH1.0 − (A510nm − A700nm) pH4.5; MM=molecular weight; FD=dilution factor; ε = molar absorptivity; 1 = correction factor.

The encapsulation efficiency (EE) and loading capacity (LC) were calculated according to the Eqs. (2) and (3):

$$EE(\%) = \frac{\text{Total (Anthocyanin nanoencapsulated)} - \text{Free (Anthocyanin)}}{\text{Total (Anthocyanin)}} \times 100 \quad (2)$$

$$LC(\%) = \frac{\text{Total (Anthocyanin nanoencapsulated)} - \text{Free (Anthocyanin)}}{\text{Total (Nanoparticles)}} \times 100 \quad (3)$$

2.6.2. Determination of size, homogeneity, and stability of nanostructures

The determination of the size distribution (nm), polydispersity index (PDI), and zeta potential (ζ) (mV) was through the dynamic light scattering (DLS) with a Zetasizer particle analyzer (Malvern®) with a fixed angle detector of 173°, the temperature of 25 °C, through a glass cuvette with square aperture, measurement position (mm) of 4.65, water dilution (1:1), refractive index 1.45, dispersant 1.330, and 1 mL of the nanostructures ^{99m}Tc-anthocyanin loading (Osvaldt Rosales et al., 2021).

2.6.3. Morphology of nanostructures

The morphology of the nanostructures was visualized through scanning electronic microscopy. Initially, samples of nanostructures were dried at room temperature, dispersed on a double carbon strip, and metalized with a platinum coating (10 nm). They were viewed in a Thermo Fisher Scientific scanning electron microscope (Quanta 650 FEG model) under a 5 kV electric field emission scan, 2.5 spots, and high vacuum mode with a second detector in an electron microscope. Magnifications of 50,000 x were used.

2.7. Molecular image, Kinect of absorption, and biodistribution of nanoencapsulated ^{99m}Tc-anthocyanin in animal

The animal model used was Balb/C mice, healthy males, 6 to 8 weeks old, 30 g of medium weight. The animals originated from the Central Bioterium – IPEN. The protocol complied with the ARRIVE guidelines (Animal Research: Reporting of *In Vivo* Experiments) and was carried out following the National Research Council's Guide for the Care and Use of Laboratory Animals through approval from the Ethics and Biosafety Committee – IPEN and approved under registration #35/22. The animals were housed (maximum 5 per cage) under standard conditions (12 h light/dark cycle, 30 – 70 % relative humidity, 20 – 26 °C) with standard palletized feed and water *ad libitum*. The animals were fasting for food for 6 h before the procedure. ^{99m}Tc-anthocyanins were administered orally by gavage into two groups: 1) free ^{99m}Tc-anthocyanins mixed with the same proportion of pectin and lysozyme as nanoparticles and 2) nanoencapsulated ^{99m}Tc-anthocyanins. Both groups had the same volumes and radioactive activity (0.4 mL and 37 MBq).

2.7.1. Molecular image of ^{99m}Tc-anthocyanin by μSPECT/CT

The images were analyzed by μSPECT/CT (Micro Single-Photon Emission Computed Tomography/Computed Tomography – Albira®) with free and nanoencapsulated ^{99m}Tc-anthocyanin (0.4 mL and 37 MBq for both groups) administered orally (gavage) as already described. During image acquisition, the animals were sedated by isoflurane 2 % in medical oxygen. The imaging protocols were 3D FOV 80 45 proj/s for μSPECT and high 400 μA 45Kev for CT. Images were processed and quantified (Standard Uptake Value – SUV %ID/g) using PMOD software (PMOD Technologies, Zürich, Zurich, Switzerland). Images were captured at predetermined times: 30 min, 1, 2, 3, 4, 6, and 24 h. To identify the route of elimination, ^{99m}Tc – anthocyanin (37 MBq) was administered intravenously (IV) (lateral tail vein), and imaging in different organs (30 min, 6, and 24 h) was observed under the same conditions already mentioned.

2.7.2. Biodistribution of ^{99m}Tc-anthocyanin in mice

The Balb/C mice received 37 MBq of ^{99m}Tc-anthocyanin or nanoencapsulated ^{99m}Tc-anthocyanin in the same radioactivity and volume by gavage for the biodistribution study. Twenty-four hours after oral administration, the animals were euthanized (Isoflurane 5 %), and the organs/tissues of interest were collected (blood, heart, lungs, liver, kidneys, spleen, bladder, pancreas, bone (femur), muscle (gastrocnemius), brain, and rinsed in phosphate-buffered saline (PBS). The structures were weighed and counted using a Perkin Elmer (Waltham, MA, USA) Wizard 2 2480 automatic gamma counter to quantify the percentage of injected dose per gram of tissue (% ID/g).

2.7.3. Evaluation of the kinetics of the nanoencapsulated ^{99m}Tc-anthocyanin absorption

To study the kinetics of anthocyanin absorption, 0.4 mL with 37 MBq of ^{99m}Tc-Anthocyanin in two different groups (nanoencapsulated and unencapsulated anthocyanins mixed with the same proportion of pectin and lysozyme) were administered by gavage. Then, the tail vein collected venous blood samples (5 μL) at 0.25 to 24 h. Blood activity was measured using a Wizard 2 2480 Perkin Elmer (Waltham, MA, USA) automatic γ counter to determine radioactivity per sample. To determine the kinetics, the radioactive activity corrected for the half-life of the radionuclide (technetium) was considered, correlating with the activity and mass injected. The area under the curve was used to determine the % absorbed in the determined time.

2.8. In silico nanostructure formation and released studies

A linear pectin chain comprising 15 homogalacturonan monomers was constructed using Maestro-Schrodinger software (Schrödinger, 2021) with the OPLS3e force field (Roos et al., 2019). The pKa values of the carboxylic groups within each monomer were determined using the Epik software (Shelley et al. 2007), revealing a consistent pKa of approximately 3.2. To explore the implications of this finding, two pH conditions were selected: pH 5.0, matching the experimental conditions for *in vitro* nanostructure formation, and pH 3.0, representing the acidic environment of the animal stomach model. Pectin chains prepared at neutral pH exhibited a total charge of 0, while those prepared at acidic pH carried a net charge of −15 (−1 per monomer). Subsequently, both pectin chains were immersed in periodic boxes filled with pre-equilibrated Single Point Charge (SPC) water molecules. A 10 ns molecular dynamics simulation was performed for thermal equilibration under NPT conditions at ambient temperature and pressure. The final frame of each simulation was retained for nanostructure construction.

Similarly, the structure of C3G was adapted from the co-crystallized molecule (PDB: 6QCH) (You et al., 2019) and energetically minimized. As C3G lacks functional groups with pKa values relevant to the pH range studied, it was modeled at pH 5.0, resulting in a positively charged ring linked to the flavylium cation. Nanostructures designated Pect15-charged (prepared with pectin chains at pH 3.0) and Pect15-neutral (prepared with pectin chains at pH 5.0) were assembled using the Packmol program (Martínez et al., 2009) according to the experimental stoichiometry of pectin: C3G (1:0.4). Each nanostructure consisted of 450 C3G monomers enclosed within a 50 Å diameter sphere, surrounded by 30 pectin chains within a 70 Å diameter outer sphere. The nanostructures were optimized using the Steepest Descent algorithms followed by the Newton-Rhapson method to ensure convergence. Subsequently, SPC water box systems were generated by embedding the nanostructures and neutralizing them with Na + and Cl- counterions, following a previous protocol reported by Bustos et al. (2023).

The systems were then subjected to triplicate 200 ns simulations under conditions similar to those used for the initial pectin chains. Interactions between pectin and C3G within each system were analyzed quantitatively and qualitatively, focusing on hydrogen bonds (HBs) and salt bridges (SBs) throughout the simulation trajectories. Additionally, the radius of gyration (Rg) was calculated for pectin and C3G to assess system compaction/extension. Finally, the release of anthocyanin over time was monitored using a protocol like that described by Valdes et al. (2024), wherein the radius of gyration and center of mass of the nanostructure was tracked over time to quantify the number of anthocyanin molecules released beyond 5 Å from the polymer.

2.9. Statistical analysis

Analyzes were performed in triplicates and expressed as mean ± SD. Statistical analysis was conducted using GraphPad Prism® software (version 10; San Diego, CA, USA). The data was analyzed using an unpaired *t*-test (multiple t-tests). Statistical significance was set at $p < 0.05$.

3. Results

The main anthocyanin identified in the enriched blackberry extract (*Rubus* spp.) by HPLC-DAD was cyanidin-3-*O*-glucoside (C3G) (Mw ≈ 449 g/mol). This identified anthocyanin corresponds to > 95 % of the total anthocyanins (Supplementary Figure S1C).

3.1. The new methodology for labeling anthocyanins with a radioactive isotope

The pertechnetate technetium (99 m) solution was eluted from molybdate (^{99}Mo) bound to a chromatographic substrate. The C3G was radiolabeled directly with metastable ^{99m}Tc in an acid solution; observing the Retention Time (RT) values before and after the reaction, it was noted that the molecule C3G had an RT of 8.1 min, technetium of 3.4 min, and after the reaction, there was a peak displacement (RT 8.7 min) demonstrating an interaction between the radioisotope and C3G (Supplementary Figures S1A–D). The degradation of the molecule C3G was not observed after the radiolabeling process nor after 24 h (Supplementary Figures S1E and F). Similarly, after the chemical complexation reaction, isolated technetium showed a significant change in the peak intensity (Supplementary Figure S1D). The ITLC indicates the radiochemical purity of the anthocyanin radiolabeling, demonstrating a value > 95 % in the formation of ^{99m}Tc-anthocyanin in two mobile phases: 100 % methyl ethyl acetone (Supplementary Figure S2A) and a mixture between pyridine: ethanol: water (Supplementary Figure S2B). ^{99m}Tc-anthocyanin was solubilized in saline solution (Fig. 1A) and in Balb/C mouse plasma (Fig. 1B) and was stable at different times (0 to 24 h), with very low detection of the free radionuclide, evidence of the absence of molecule degradation and confirming the stability of the radiochemical labeling.

An *in silico* approach was employed to simulate the potential structure of the complex formed between the radioisotope ^{99m}Tc and anthocyanin (C3G) (Supplementary Figure S3). Ten potential complex structures were proposed, considering the nature of ^{99m}Tc complexes and the experimental conditions involved in labeling anthocyanin with the metal (Supplementary Table S1). Fig. 2A and B depicts the complex exhibiting the lowest potential energy, indicating the most stable optimized structure. This configuration is suggested as a plausible outcome in the radiolabeling process of anthocyanin with ^{99m}Tc. Due to the low amount produced for the experiments and the limitation in using radioactive activity per sample, no other chemical characterization was done besides chromatographic separation with radiometric detection (Supplementary Figure S1D).

3.2. Chemical-structural properties of ^{99m}Tc-anthocyanin-loading nanostructures

The chemical-structural properties of nanostructures containing ^{99m}Tc-anthocyanin were analyzed to understand their colloidal characteristics and stability. The average diameter of the nanostructures was 222.4 nm (±72.1 nm), and the PDI was 0.1 (±0.0) (Supplementary Figure S4A). The identified zeta potential was –31.7 mV (±5.32 mV)

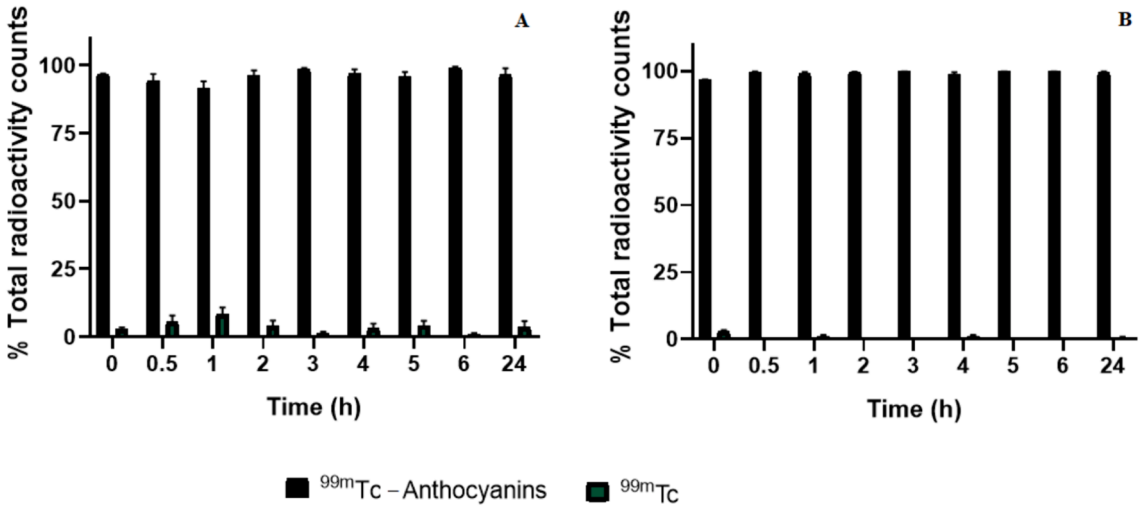

Fig. 1. **A**. Stability of ^{99m}Tc – anthocyanin in saline solution. **B**. Stability of ^{99m}Tc-anthocyanin in mice plasma. The percentage of radioactivity at different times.

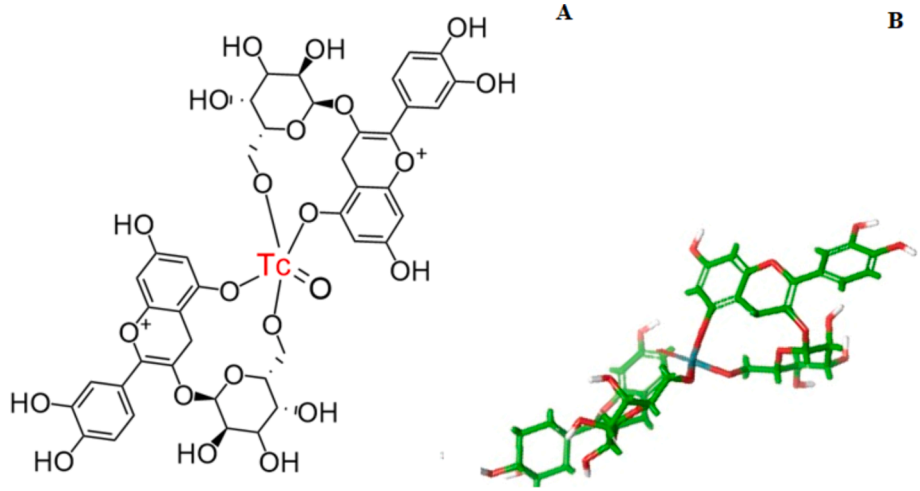

Fig. 2. An *in silico* model was proposed based on the lower energy (−4014.99) involved and the molecular stability forming the ^{99m}Tc – C3G. **A.** Two-dimensional and **B**. Three-dimensional model.

(Supplementary Figure S4B). The encapsulation efficiency (EE) was 75 % ± 5.0, and the loading capacity (LC) was 15 % ± 1.0. Fig. 3 shows the morphology of the nanostructures. They enabled the observation of adequate colloidal stability, homogeneity, and efficient encapsulation and loading of anthocyanin.

3.3. Study of the biological distribution of nanoencapsulated ^{99m}Tc-anthocyanin in mice

The image of free ^{99m}Tc-anthocyanin after intravenous (i.v.) administration in mice (Fig. 4A–D) indicated the affinity of ^{99m}Tc-anthocyanin in different tissues (30 min, 6, and 24 h) and organs directly involved in metabolism (liver) and excretion (kidneys and bladder). Not observing signals in other tissues does not mean radiolabeled compounds did not reach the tissue since the detectors can only be calibrated to higher radiation intensities.

Fig. 5A–C show the image of free ^{99m}Tc-anthocyanin after oral ingestion (gavage) and the nanoencapsulated ^{99m}Tc-anthocyanin at different times: 30 min, 6, and 24 h after administration. Fig. 5D–F refer to quantifying radioactivity (%) in the stomach and small and large intestines. The molecular image indicates the difference in the flow of unencapsulated and nanoencapsulated ^{99m}Tc-anthocyanin in the gastrointestinal tract. The nanoencapsulated molecule has a slower transit; after 24 h of administration, it can still be detected, suggesting a gradual emptying of the stomach to the intestine. Supplementary Figure S5 shows images captured at times 1, 2, 3, and 4 h after gavage.

The biodistribution was detected in different animal structures, comparing free (unencapsulated) with nanoencapsulated ^{99m}Tc-anthocyanins. The quantification (%) in various organs/tissues was done in the blood, heart, lung, liver, kidney, bladder, pancreas, bone, muscle, and brain (Fig. 6A). The absorption kinetic study (Fig. 6B) was conducted in mice to verify the *in vivo* difference between nanoencapsulated ^{99m}Tc-anthocyanin and free ^{99m}Tc-anthocyanin. The absorption (gastric and intestinal) in the body and the excretion kinetics of nanoencapsulated and free ^{99m}Tc-anthocyanin were considered. The statistically significant differences between the two groups are verified in 0.75, 1, 2, 3, and 24 h after the oral administration. The AUC (Fig. 6C) indicates that $1.317 \times 10^{-5} \pm 8.817 \times 10^{-7}$% I.D./μg of nanoencapsulated ^{99m}Tc-anthocyanin was absorbed in 24 h, while the free ^{99m}Tc – anthocyanin was $1.058 \times 10^{-5} \pm 1.331 \times 10^{-6}$ % I.D./μg. Values correspond to $5.65 \times 10^{-6} \pm 9.60 \times 10^{-7}$% and $2.96 \times 10^{-6} \pm 8.32 \times 10^{-7}$% injected mass (μg), respectively. This data demonstrates that anthocyanin, when nanoencapsulated, had a more efficient absorption, and the amount detected in the blood indicates that the encapsulation process significantly favored bioavailability and tissue delivery.

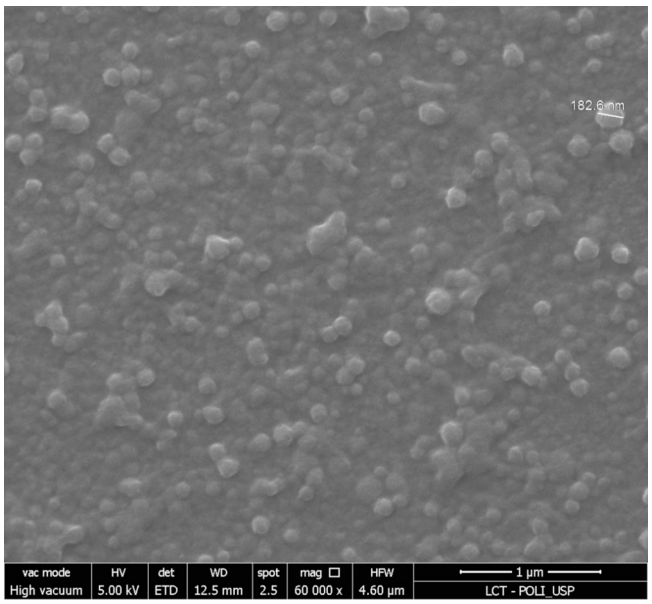

Fig. 3. Morphological analysis of dried nanocapsules with anthocyanins loaded. Scanning electron microscopy images by electric field emission, Quanta 650 FEG microscope, magnification of 60,000 ×.

Fig. 7 summarizes the approach used in this study to detect nanoencapsulated ^{99m}Tc-anthocyanin and compares it with the unencapsulated form. Based on the results of the molecular image (Fig. 5A–F) and the biodistribution (Fig. 6A and B), it can be observed a slower flow in the gastrointestinal tract resulted in better absorption, leading to the detection of radioactivity in different tissues in nanoencapsulated samples. In contrast, the molecule without encapsulation has a rapid transit from the stomach to the intestine and was not detected in most of the tissues analyzed, indicating limited bioavailability.

3.4. Computational insights into the pH-dependent release behavior of nanoencapsulated-cyanidin-3-O-glucoside complex

Computational simulations were conducted to explore potential release mechanisms for the nanoencapsulated-C3G complex over time, as it can interact in a neutral-alkaline environment (simulating blood and intestine) and an acidic pH environment (simulating stomach). The *in silico* experiments were done without considering the C3G radiolabeling to simulate the natural physiological conditions and a possible final product. The findings reveal notable distinctions in the compaction, intermolecular interactions, and release patterns of nanostructures elaborated under acidic (pH 3.0) compared to pH 5.0 (Fig. 8A and B). The final snapshots of our simulations reveal distinct nanostructures' sphericity depending on the pH environment. Notably, C3G molecules exhibit enhanced association with the nanostructures under acidic conditions compared to neutral pH (Fig. 8A). The radius of gyration (Rg) of C3G molecules (Supplementary Figure S6A) indicates a greater degree of compaction, with an average difference of over 5 Å between pH 3.0 and 5.0. Pectin chains tend to compact more effectively at pH 5.0 (Fig. 8B), as evidenced by their Rg values (Supplementary Figure S6B), which show approximately 5 Å more compaction than pH 3.0.

Analysis of intermolecular bonds reveals a substantial increase in hydrogen bonds (HBs) at acidic pH, with nearly double the average number of interactions compared to neutral pH (467 ± 34.70 HBs versus

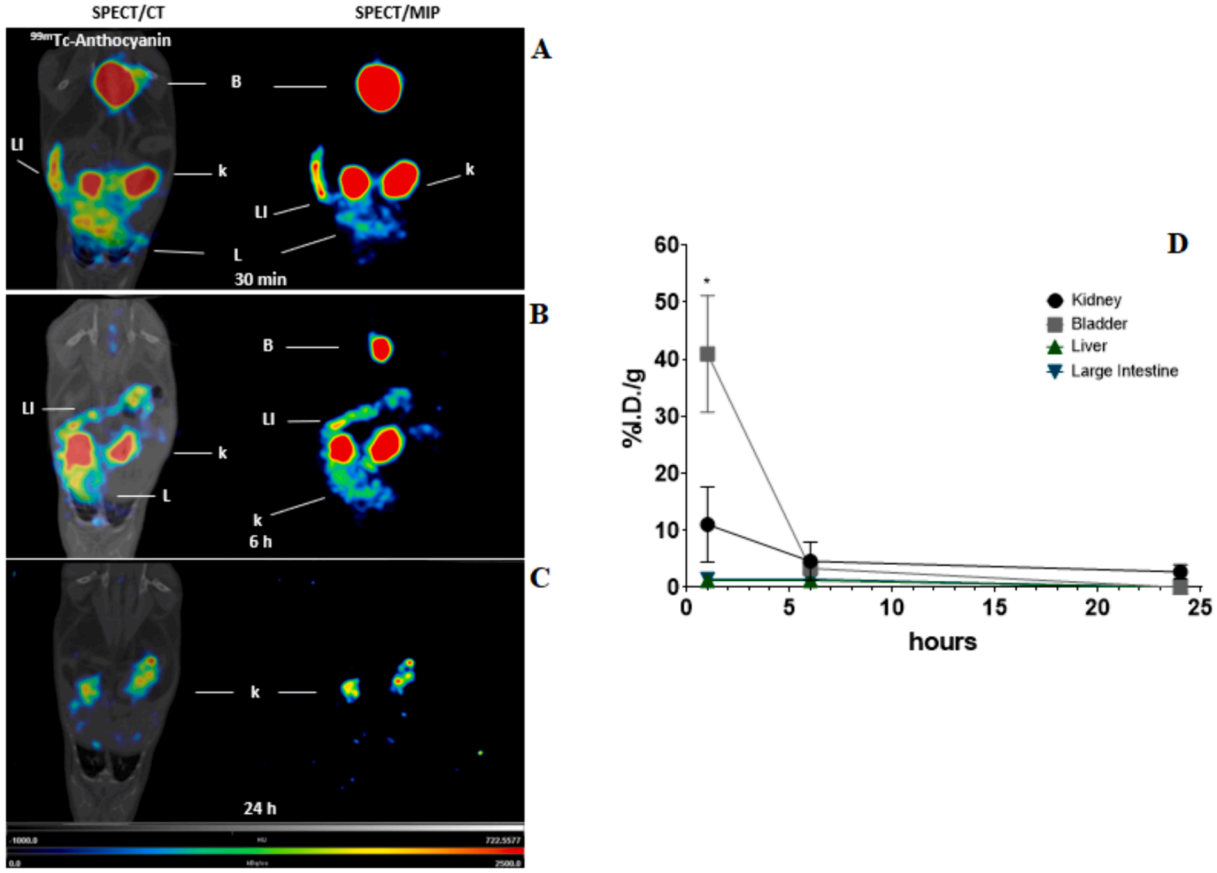

Fig. 4. Biodistribution of ^{99m}Tc-anthocyanin after intravenous administration in mice, the bioactive compound in different organs/tissues. **A.** 30 min, **B.** 6 h, and **C.** 24 h after oral administration. **D** Represents the %ID/g quantification of ^{99m}Tc − anthocyanin in the kidney (K), bladder (B), liver (L), and large intestine (LI) at different times. *Statical differences between two groups using *t*-test ($p < 0.05$) ($n = 3$).

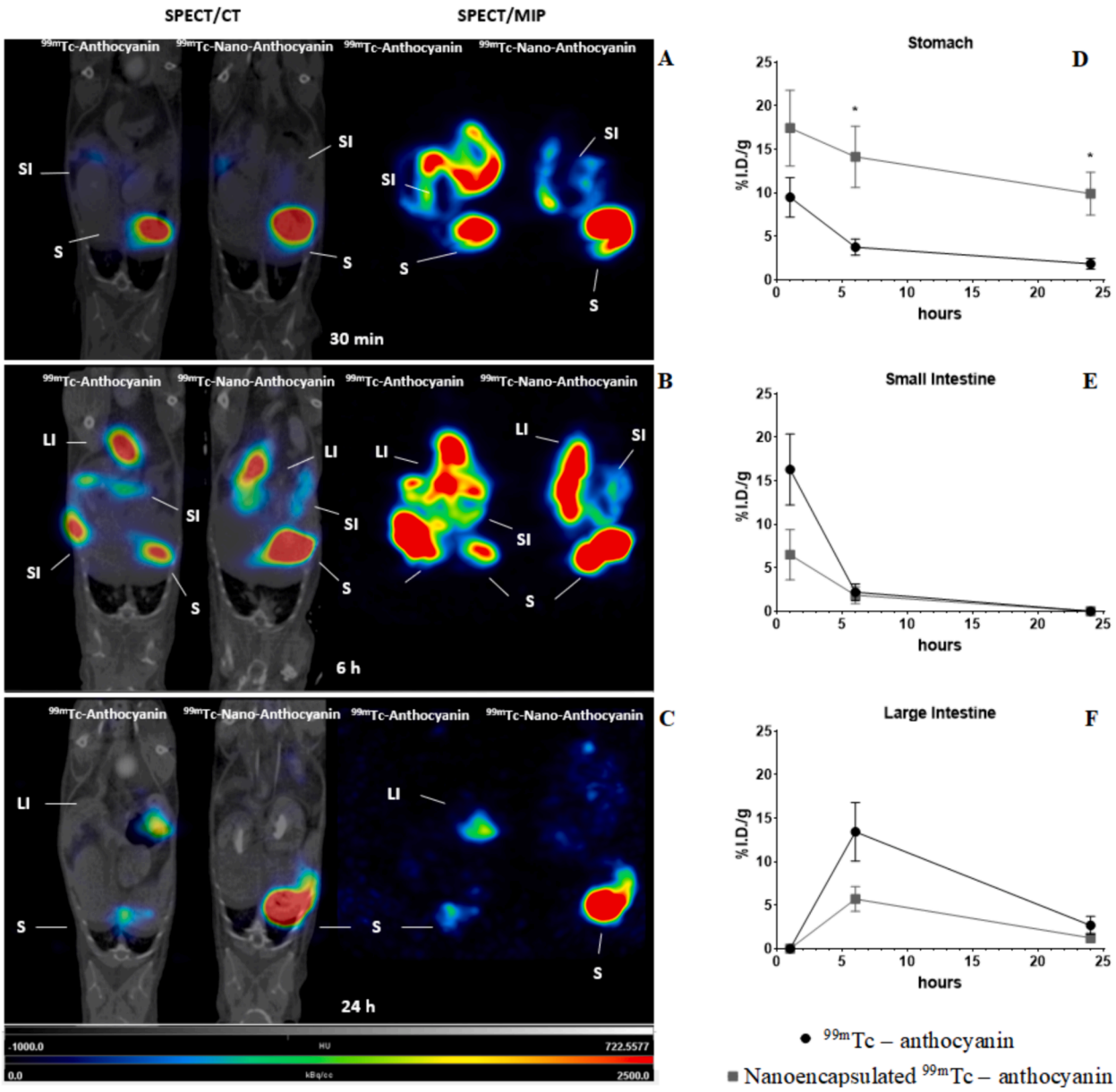

Fig. 5. Visualization of intestinal flow after oral ingestion of nanoencapsulated ^{99m}Tc-anthocyanin and the free molecule (unencapsulated). **A**. 30 min, **B**. 6 h, and **C**. 24 h after oral administration. **D-F** The %ID/g quantification of ^{99m}Tc-anthocyanin in the stomach, small intestine, and large intestine at different times (30 min, 6, and 24 h). Data corresponded to three independent experiments (n = 9). μSPECT/CT: Single-Photon Emission Computed Tomography/Computed Tomography. MIP: Maximum Intensity Projection. S: stomach; LI: large intestine; SI: small intestine. *Significant statistical differences between two groups using Student's *t*-test ($p < 0.05$).

201 ± 15.50 HBs) (Fig. 8C). However, no significant salt bridges (SBs) are observed in systems at pH 5.0 (Fig. 8D). Nanostructures subjected to neutral pH have a markedly higher release of C3G molecules throughout the simulation, releasing nearly ten times more C3G on average than acidic conditions (31.4 ± 3.98 versus 2.94 ± 0.85) (Fig. 8E). Finally, we observed that nanostructures subjected to less acidic pH tend to release, on average, almost 10 times more C3G molecules throughout the simulation time (31.4 ± 3.98) than at acidic pH (2.94 ± 0.85).

4. Discussion

4.1. Radiolabeled anthocyanins, stability, and nanostructure characterization

The identified anthocyanin (C3G) corroborates previous studies with the same analytical parameters for blackberries (Rosales et al., 2023b; Osvaldt Rosales et al., 2021). The new methodology for complex formation with anthocyanins and technetium (^{99m}Tc-anthocyanin) was effective with radioactive and molecular chemical stability. Anthocyanin (acidic solution) was radiolabeled through a direct electrophilic substitution reaction using a reducer agent ($SnCl_2$), a complex formation reaction between the metal and the molecule. ^{99m}Tc is reduced from the 7^+ to 3^+ state to create the corresponding complex, while Sn is oxidized from the 2^+ state to 4^+. The ^{99m}Tc-anthocyanin was obtained with a maximum labeling yield of 95 ± 0.0 % with excellent physiological stability *in vitro* (saline and mice plasma) for 24 h. The complexation between radioactive isotope and anthocyanin acquired an adequate and efficient radiochemical purity.

Anthocyanins are complex hydrophilic compounds formed by aromatic rings linked to a flavylium cation (AH^+) and different sugar

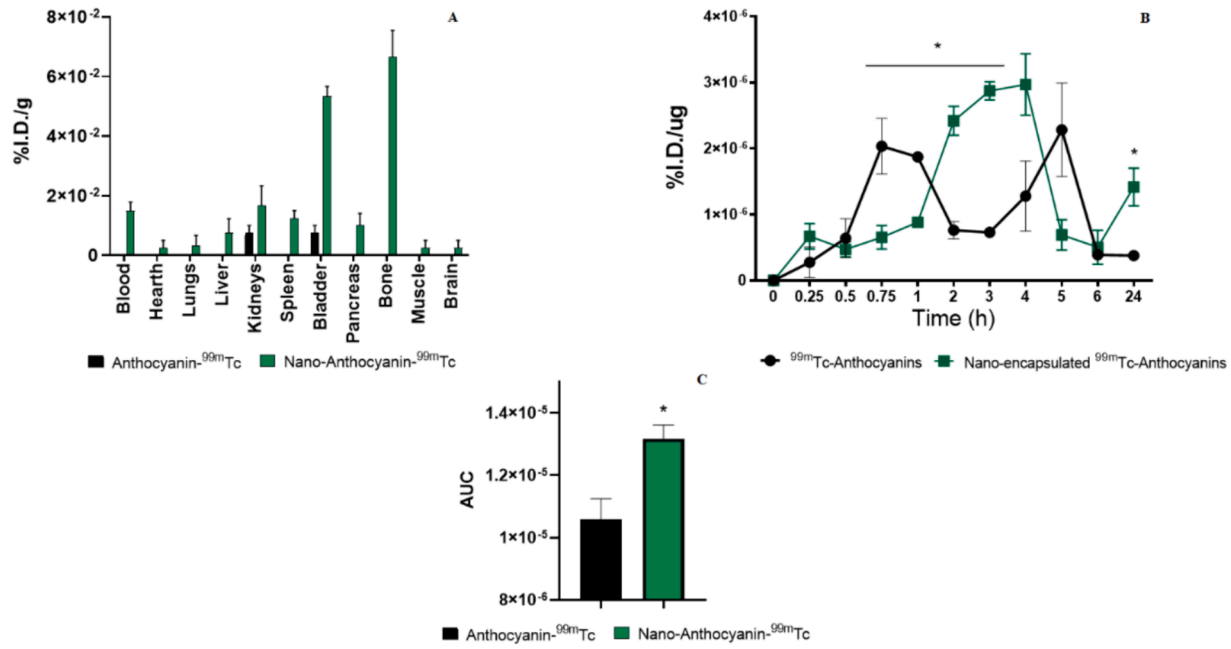

Fig. 6. **A**. In mice, free molecules compared to nanoencapsulated ^{99m}Tc – anthocyanin. Quantification in different organs/tissues indicates the biodistribution profile in animals' internal organs, which suggests the uptake of ^{99m}Tc-anthocyanins after intestinal absorption in 24 h ($n = 10$). **B**. Kinetic absorption of ^{99m}Tc – anthocyanin (nanoencapsulated versus free ^{99m}Tc – anthocyanin molecule) ($n = 10$) in 24 h. **C**. Area under the curve, amount of ^{99m}Tc – anthocyanin absorbed in 24 h. Data are expressed as means ± SD. *Statical differences between two groups using *t*-test ($p < 0.05$). I.D. Injected Dose ($n = 10$).

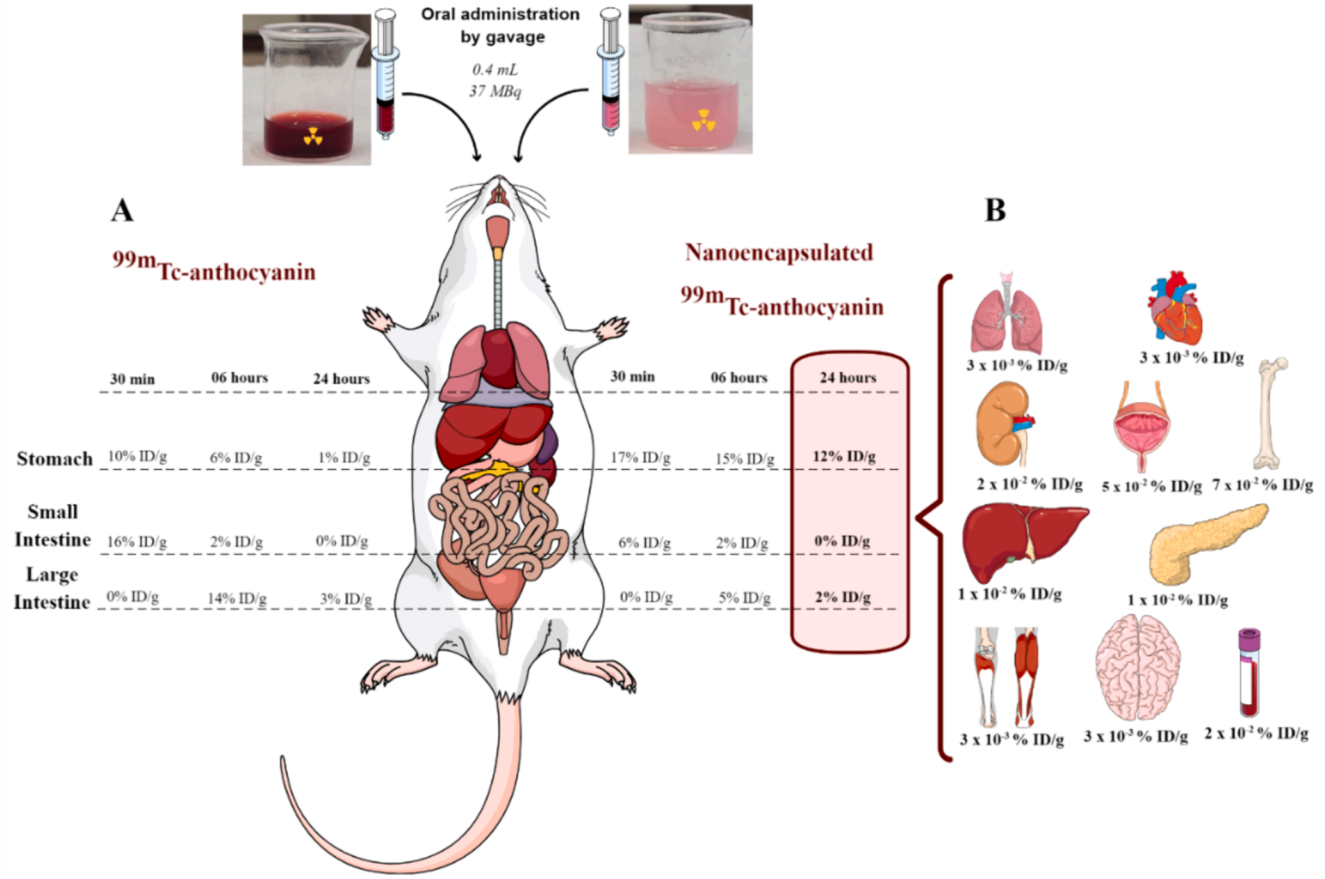

Fig. 7. Approach for determining biodistribution in mice. **A.** Detection of nanoencapsulated ^{99m}Tc-anthocyanin compared to free ^{99m}Tc-anthocyanin in the gastrointestinal tract flow after 30 m, 6 h, and 24 h of oral ingestion, according to Fig. 4 D-F. **B**. Nanoencapsulated ^{99m}Tc-anthocyanins detected in different tissues after 24 h (biodistribution), as shown in Fig. 5 A-B. I.D. Injected Dose (%). The figure was created with Mind the Graph (https://mindthegraph.com) (accessed on 30 June 2024).

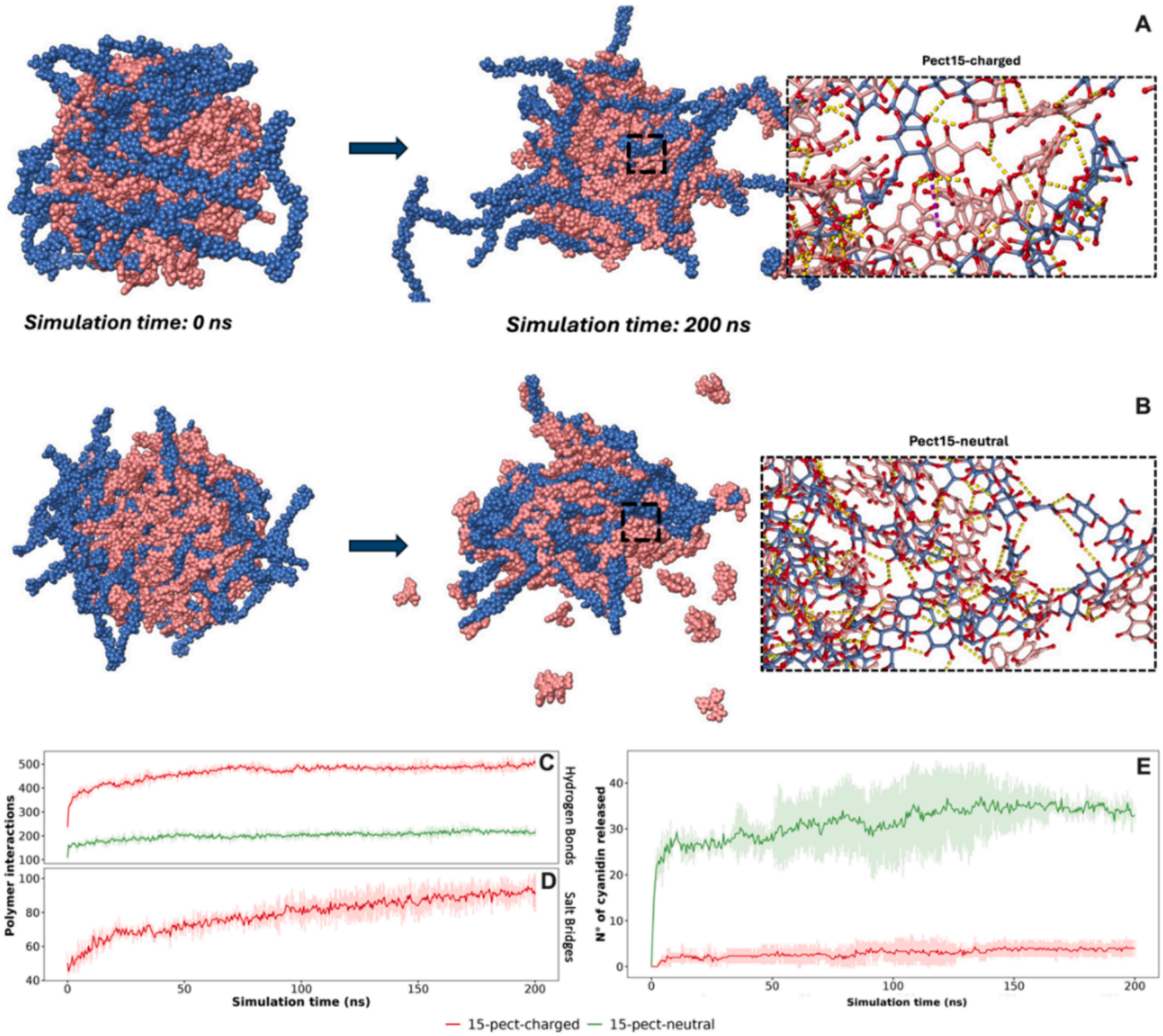

Fig. 8. Computational analysis of nanostructures formation and C3G. **A.** The initial (0 ns) and final step of simulation (200 ns) for the nanostructures systems denoted as Pect15-charged (at pH 3.0) and **B.** Pect15-neutral (at pH 5.0); an approach to the intermolecular interactions between pectin-Cya. The yellow dotted lines represent hydrogen bonds and the purple one's salt bridges. The pectin chains/monomers are depicted in blue, and the C3G molecules are pink. **C.** and **D.** The number of intermolecular hydrogen bonds and salt bridges (mean ± S.D.). E) Number of C3G molecules released over time. The thick central line represents the average of the three replicates, and the variation in pale color represents the standard deviation (S.D.). Note that **C**, **D**, and **E** use the same color scheme for Pect15-charged systems in red and Pect15-neutral systems in green. (For interpretation of the references to color in this figure legend, the reader is referred to the web version of this article.)

molecules (Tena et al., 2020). *In silico* approaches in the structure's design, they have indicated the probable complex developed by the interaction between C3G and the transition metal ^{99m}Tc due to the most excellent stability among the proposed complexes. Molecular modeling determined all possible structures of ^{99m}Tc-anthocyanin and confirmed the effective radioactive labeling process, evidenced by the lowest potential energy involved (Felgines et al., 2010). The ^{99m}Tc-anthocyanin was nanoencapsulated in a polysaccharide and protein structure through molecular self-assembling, forming stable, spherical, and homogeneous nanostructures. The nanostructures had appropriate characteristics for diameter (~200 nm), homogeneity (PDI<0.2), and colloidal stability with a zeta potential of ~ –32 mV (Fang et al., 2020), with excellent encapsulation efficiency (75 %) and loading capacity (15 %) (Salah et al., 2020).

4.2. Biodistribution of ^{99m}Tc-anthocyanin after oral ingestion in mice and their absorption kinetics

Anthocyanins are bioactive compounds with high antioxidant activity and immunomodulatory effects (Tena et al., 2020). The targeted delivery of this bioactive compound has therapeutical potential to benefit circulatory (Mozos et al., 2021), endocrine (Millar, Duclos & Blesso, 2017), digestive (Ayvaz et al., 2023), urinary (Li et al., 2021), nervous (Zhong et al., 2023), bones (Quek et al., 2023), and immunological systems, and regulates energy metabolism and insulin sensitivity (Yao et al., 2021). Despite advantageous properties, molecular instability reduces biological effects; the action of enzymes, microbiota, and intestinal pH compromises molecular integrity, limits absorption, and decreases bioaccessibility and bioavailability (Marques et al., 2018).

Current research into the bioactivity after ingestion of anthocyanins shows that *in vivo* concentrations after oral ingestion are insufficient to obtain the same effects comparable to *in vitro* studies (Tarone et al. 2021). On the other hand, nanoencapsulation techniques can improve molecular stability, promoting effective absorption and release in the physiologically active sites (Rosales & Fabi, 2022; Salah et al., 2020).

Our study demonstrated an *in vivo* approach in which nanoencapsulated anthocyanins are gradually released in the gastrointestinal tract. Here, nanostructures loading ^{99m}Tc-anthocyanins were administered orally to understand the biological pathway, time of retention, and excretion from the body. Nanostructures provide more significant absorption of molecules and deliver targeted to organs/tissues more efficiently than free molecules (unencapsulated). Furthermore, a new methodology was successfully developed to radiolabel the anthocyanin directly with the ^{99m}Tc isotope, resulting in a stable complex for biological distribution studies.

Molecular imaging was essential to elucidate the biological destination of nanoencapsulated ^{99m}Tc-anthocyanins after oral ingestion and was used for the first time in literature for this purpose. Moreover, the biodistribution/accumulation at different organs/tissues and the elimination of these bioactive compounds indicate that the nanoencapsulation process influences gastric and intestinal absorption, and the nanostructures can protect anthocyanin against intrinsic gastrointestinal factors, promoting effective uptake and improve the reach of specific biological structures (Rosales et al., 2022). Especially for 6 to 24 h, it is notable that nanoencapsulated ^{99m}Tc-anthocyanin was gradually released from the stomach into the intestine. Both nanoencapsulated and free anthocyanins showed similar behavior in the small intestine. However, free ^{99m}Tc-anthocyanin was detected more significantly in the large intestine, indicating possible lower absorption and considerable fecal excretion. Simultaneously, there was a substantial amount of the molecule from the nanostructure in internal organs and tissues. Previous studies suggest that bioactive compounds within nanocomplexes could effectively delay the release in the gastrointestinal tract according to specific physiological stimuli, such as pH range variations and microbiota action (Zhao et al., 2020).

Rosales et al. (2023b), in a recent digestion simulation study using the Infogest method (Brodkorb et al., 2019), observed that C3G, when nanoencapsulated, was less chemically degraded when compared to the free molecule (unencapsulated). Additionally, the release of anthocyanin from the nanostructures in the gastrointestinal tract *in vitro* was gradual. The physicochemical characteristics of the nanostructure, analyzed through SEM and DLS (size, PDI, and zeta potential), indicated that in the gastric phase (acid pH), there was an increase in zeta potential modulus (from –32 mV to –5 mV) and an increase in diameter and PDI, which probably occurs by protonation of the nanostructures and consequent transitory aggregation. However, when it reached the small intestine (neutral pH), there was a decrease in the zeta potential, returning to the initial value (–32 mV), and with electrostatic repulsion of the nanostructures, the diameter and PDI also returned to the original values. Pectin covers the nanostructure, and the carboxylic acids not linked to anthocyanin are deprotonated by increased pH, exceeding the protein (positive charge) protonation. The predominance of negative charges around the nanostructures leads to electrostatic repulsion, resulting in stability (no aggregation) in the intestine. The changes in the physical–chemical characteristics of the nanostructures in the stomach environment (acidic) and intestinal (neutral) possibly induced a gradual and decelerated gastric emptying and provisioned release in the intestine (Antonov et al., 2021; Osvaldt Rosales et al., 2021).

In our study, we identify a significant difference in the retention time of nanoencapsulated anthocyanins compared to free molecules. It is noted that when nanoencapsulated, the molecules remain in the body for a more extended period, especially in the stomach, which could induce gastric absorption. Furthermore, emptying from the stomach to the intestine was delayed by the characteristics of the nanostructure on the acidic pH. In the intestine, neutral-alkaline pH gradually released anthocyanins. The nanoencapsulation provided a controlled release of anthocyanin and more time for gastrointestinal transit, which induced a local prolonged effect. Both behaviors in different physiological pH during digestion were previously described during the INFOGEST protocol (Rosales et al., 2023b) and corroborated during the *in silico* analyses shown herein. At the same time, the nanostructures may have been absorbed entirely, and the encapsulated molecules were released into the cell interior, facilitating the migration to the bloodstream and internal organs.

Polysaccharides have essential characteristics for the delivery of anthocyanin. For example, pectins are hydrophilic molecules with degradable and fermentable structures and can pass intact through the gastrointestinal tract, resisting digestive factors and reaching more distal portions of the intestine. When associated with other compounds like proteins they can generate a complex polymeric network of interconnected and hydrophobic core, forming a stable barrier to prevent the penetration of polar reactive compounds to attack entrapped anthocyanins (Rosales & Fabi, 2023). As a biomaterial for targeted delivery, pectin has properties of bio-specific interactions, adhesiveness to the intestinal mucosa, and a capacity for releasing controlled encapsulated compounds according to specific physiological stimulation or cellular interaction. If released from the pectic nanostructure into the intestinal lumen, anthocyanins can be absorbed by active transport or passive diffusion processes through the intestinal epithelium. However, another hypothesis refers to the absorption of pectic nanostructures through mechanisms that involve the paracellular route and endocytosis of intestinal epithelial cells and release into the cell interior or systemic circulation to be distributed to tissues (Zhang et al., 2020).

The complex metabolism of anthocyanins has yet to be fully elucidated in the literature, and limited information makes it difficult to understand their fate from ingestion to elimination. Despite this, the low bioavailability of anthocyanins has been frequently reported and constitutes a challenge to overcome (Braga et al., 2018). In this regard, our results can contribute to revealing strategies for increasing the absorption and bioavailability of anthocyanins, which should be applied to other labile compounds.

In recent years, studies have been carried out to comprehend the absorption of anthocyanins *in vivo* (humans and animals) through different methodologies, and the results suggest that the proportion of total anthocyanins absorbed in intact form is less than 1 % of the quantity ingested (Chatterjee et al., 2021). Chemical properties determine the *in vivo* stability of anthocyanins and their derived products, influencing transport, association with the biomatrix, absorption, deposition in the body, and bioactivity (Kalt, 2019; Van de Velde et al., 2018). Due to the extensive chemical modification of anthocyanins throughout the gastrointestinal tract, the absorption of intact molecules is reduced, and the products of their catabolism can be absorbed or excreted via the renal system and feces (Braga et al., 2018). In the stomach, these compounds are known to be stable due to the acid environment (pH 1.5–2), with a predominance of the flavylium cation (stable form) that can be absorbed by the gastric epithelium (around 1 %–10 % total absorption) (He et al., 2022). The remaining molecules – most anthocyanins – are absorbed in the intestine. In the small intestine (pH 7.4–8), mainly in the jejunum, glycosylated anthocyanins are absorbed via glucose transporters (active absorption by SGLT1 and GLUT2) (Oliveira et al., 2019); the aglycone form is absorbed by passive transport. In the small intestine, these compounds undergo deconjugation reactions. In enterocytes, phases I and II of metabolism, such as methylation, glucuronidation, and sulfation, are catalyzed by UDP-glucuronosyltransferase, sulfotransferases, and catechol-*O*-methyltransferase (Verediano et al., 2021). Despite being poorly absorbed, anthocyanins are quickly detected in the blood after ingestion and circulate in the bloodstream in intact, methylated, glucuronide, and sulfate-conjugated forms and are excreted in the urine and feces (Hahm et al., 2022). Our results corroborate this absorption flux of free anthocyanins (Fig. 5A–F).

Unabsorbed anthocyanins and their metabolites pass into the large intestine (pH 7.4–8) to be metabolized by colonic microbiota (Hou et al., 2021; Rosales et al., 2022). Most metabolite absorption occurs during the gut biotransformation, and some unabsorbed metabolites and anthocyanins are excreted in the feces. The hydrolysis, reductions, dihydroxylation, demethylation, decarboxylation, and ring fission of the anthocyanin's aromatic structures occur in the colon. Intestinal bacteria and the integrity of intestinal villi have a fundamental role in metabolism; the degradation process results from conversion steps catalyzed by bacterial enzymes in the host's colon. Initially, structural loss occurs with deglycosylation and the formation of compounds such as cyanidin (aglycone) and low molecular weight catabolites (such as phenolic acids and other phenols) (Verediano et al., 2021). Phenolic acids can be absorbed by active or passive transport into the colon and phase II of metabolism in colonocytes. The anthocyanins and their metabolites are transported to the liver via the portal system when absorbed. The hepatocytes metabolize in phase II through conjugation (glucuronidation, sulfation, acylation, and methylation reactions) (Braga et al., 2018). After absorption, they are biodistributed throughout tissues/organs, transported to the enteric system via the bile duct, and removed by urinary and fecal excretion (Hahm et al., 2022). The concentration in blood plasma after oral ingestion is very low (nM range); despite this, C3G and its derivatives have already been detected in tissues such as the stomach, small intestine, liver, kidney, brain, and lung quickly after oral administration, and maintain in the body for a short time (Braga et al., 2018). The complex biological mechanism affects the molecular integrity and absorption of anthocyanin. As reported in our study through molecular imaging and biodistribution analyses, the unencapsulated anthocyanin 24 h after oral administration was not detected in several organs and blood, and its excretion was rapid, confirming the low bioavailability.

^{99m}Tc-anthocyanins from the nanostructures were transported through the vascular system and biodistributed to various organs and tissues, such as the liver, heart, brain, bone, pancreas, muscle, and lung; the main route of elimination was urinary (bladder and kidneys). The results indicate the gastrointestinal tract's maximum uptake of ^{99m}Tc-anthocyanin was $5 \pm 4 \times 10^{-2}$ % ID/organ in the bladder (elimination) after 24 h of gavage. Anthocyanin delivery was evidenced in other tissues in the animal model; the radioactive uptake of ^{99m}Tc-anthocyanin from nanostructure in bone tissue was $7 \pm 1 \times 10^{-2}$ % ID/organ and in kidney was $2 \times 10^{-2} \pm 9 \times 10^{-3}$ % ID/organ; the absence of detection of the free molecule in the respective organ/tissues indicates the disparity in biodistribution between the two forms (nanoencapsulated and unencapsulated). Similarly, the uptake of ^{99m}Tc – anthocyanin from nanostructures in the liver ($1 \pm 1 \times 10^{-2}$ % I.D./organ) and the lack of detection of the free molecule reinforced the difference in the biological distribution. Despite the low amount of labeled nanoencapsulated anthocyanins used in the experiments, radiolabeled compounds were detected in blood, pancreas, brain, heart, and lung structures after 24 h of the nanoparticle ingestion. At the same time, ^{99m}Tc-anthocyanin, when administered in unencapsulated form and the same amount as the nanoencapsulated counterpart, was undetected in those organs. Nanoencapsulated ^{99m}Tc-anthocyanin circulating in the blood ($2 \pm 1 \times 10^{-2}$ % I.D./organ) after 24 h of oral administration may indicate that the nanostructures were gradually absorbed into the gastrointestinal tract. The unencapsulated ^{99m}Tc-anthocyanin was not detected in the liver and blood, demonstrating differences in the absorption kinetics against the nanoencapsulated ^{99m}Tc-anthocyanins. In this way, 24 h after oral administration, the bladder accumulated more nanoencapsulated ^{99m}Tc-anthocyanin when compared to the free molecule group, indicating that the excretion process was delayed. As an overall image analysis, the nanostructures maintained the bioactive compound in the animal body for a longer time, as the μSPECTCT/CT demonstrated.

The results showed herein indicate nanostructures can improve the bioaccessibility of bioactive compounds due to the coating's protection through the digestive tract. Other properties, such as mucoadhesion, may be involved in the prolonged retention time of nanostructures in the stomach and the intestine mucous membranes (Hahm et al., 2022). The images and biodistribution were crucial to understanding the gradual and pH-responsive release of ^{99m}Tc-anthocyanin from the nanostructure.

Firstly, we investigated the kinetic characteristics of intravenous anthocyanins to reduce interindividual variability in gastrointestinal absorption and understand molecular-tissue affinity and elimination route. The liver (metabolism), kidney, and bladder (elimination organs) were detected for anthocyanin from 30 min to 6 h. Due to high kidney detection, the free molecules were eliminated via renal excretion. Similarly, a recent study evaluated the intravenous administration of anthocyanin monomers and verified that the anthocyanins were distributed rapidly and eliminated in less than 5 h (Chen et al., 2023).

In our experiments, the absorption kinetics after oral ingestion indicated a rapid and non-linear absorption of the unencapsulated radiolabeled anthocyanin; after 0.75 h, the radiolabeled molecules were detected in the animal's blood. When nanoencapsulated, radiolabeled anthocyanin significantly increased absorption due to higher radioactive concentration in the blood for a longer time. For nanoencapsulated ^{99m}Tc-anthocyanin, gradual absorption was observed 3 h after administration; the maximum significant peak was $2.87 \times 10^{-6} \pm 1.96 \times 10^{-7}$% I.D./μg. After 24 h of ingestion, the absorbed ^{99m}Tc-anthocyanin from nanostructures showed higher levels than the free anthocyanins group, with a $1.41 \times 10^{-6} \pm 2.86 \times 10^{-7}$% I.D./μg. A similar effect was observed for blood analysis after 24 h of the biodistribution, indicating a substantial amount of circulating ^{99m}Tc-anthocyanin.

In vivo research (rats and mice) indicates a high variability (10 min to 2 h) between ingesting C3G and detecting the molecule in the systemic circulation (Sandoval-Ramírez et al., 2018). The C3G in plasma and different tissues from 0.14 to 14 μM depends on the amount of oral intake, source, analysis methods, and animal models. A study of oral administration of C3G labeled isotope had maximum rates of ^{13}C elimination achieved 30 min after ingestion and rapidly observed less bioavailability in the plasma (Czank et al., 2013). Another study with ^{13}C-labeled C3G observed a concentration between 0.14 and 0.334 μM in the plasma until 1.8 h. Another research observed that the maximum concentration in plasma was 14 μM at 45 min in rats after oral ingestion (Chen et al., 2020). These studies reinforce that free anthocyanin has a rapid metabolism, excretion, and limited bioavailability.

The insufficient absorption of unencapsulated ^{99m}Tc-anthocyanin after oral ingestion and the low concentrations in plasma – compared to nanoencapsulated ones – can be attributed to its unstable chemistry and diverse formation of metabolites. Properties like molecular size, chemical form and polarity, glycoside presence, and possible phase 2 conjugates give rise to a chemically diverse set of intermediates (Kalt, 2019). Metabolites, such as phenolic acids, may be exhibited in organs; however, identification and quantification are not as precise due to the wide variability of metabolites generated from the degradation of anthocyanins and the limitations in current analytical methods. Furthermore, current analytical methods do not accurately confirm whether the anthocyanin molecule was delivered in nanoencapsulated form or already released.

Nanoencapsulated anthocyanins based on casein and carboxymethyl cellulose were orally administered to mice. Through fluorescence images of the gastrointestinal tract at different times, it was possible to observe that the intensity in the intestine increased initially, reaching its highest level after 4 h of administration and indicating a possible gradual release and accumulation in the stomach to the intestine. After 24 h, lower intensity was detected in the intestine, suggesting a potential delay in anthocyanin excretion and the protective effect of nanoencapsulation (Salarbashi et al., 2020).

Understanding the tissue biodistribution of nanoencapsulated anthocyanins is essential to identify mechanisms for future health effects and to improve the absorption of integral molecules with a release targeted to some organs. Some studies have identified (low concentrations)

anthocyanins in animals' liver, blood, kidney, brain (Sandoval-Ramírez et al., 2018), bladder, heart, and lungs. In our study, despite the radiation activities detected in all those organs, a significant quantity of nanoencapsulated ^{99m}Tc-anthocyanin was detected in the bones. The regulation of osteoblast differentiation is an effective therapeutic target for accelerating bone regeneration in osteopenic conditions (Salhotra et al., 2020). Anthocyanins have recently been identified as promising compounds for bone regeneration due to molecular mechanisms that promote osteoblast differentiation and inhibit the formation and differentiation of osteoclasts. In future studies, this fact provides new perspectives to explore the therapeutic use and application of nanoencapsulated anthocyanins in suppressing bone loss and supporting treatment for fragility fractures and osteoporosis (Quek et al., 2023). However, conducting further *in vitro* and *in vivo* tests is crucial to establish doses, administration periods, and simultaneous ingestion of nanocapsules loading anthocyanin with food components and oral administration associated with drugs. These tests can provide practical guidelines for the potential therapeutic use of nanoencapsulated anthocyanin. In addition, clinical studies are strongly recommended to corroborate these findings and explore all mechanisms involved in tissue absorption.

4.3. Impact of the physiological pH on nanostructure behavior and anthocyanin release in silico

After the *in vivo* analyses and observations of differences in absorption and retention time in the animal body, it was necessary to understand the effect of the encapsulating matrix on the release of anthocyanin through the gastrointestinal tract. Based on computational models, the impact of pH dependence on nanostructure behavior was studied with non-radiolabeled anthocyanins. The observed differences can be attributed to the presence or absence of charge within the pectin homogalacturonan monomers. In acidic environments (stomach simulation), electrostatic attractions between positively charged C3G molecules and negatively charged pectin chains promote nanostructure compaction. However, the electrostatic repulsion within the negatively charged pectin chains hinders their compaction, consistent with previous findings (Pieczywek et al., 2020). In contrast, the nanoparticle system in alkaline pH lacks a net negative charge in pectin chains, preventing electrostatic interactions and resulting in less effective compaction and the absence of salt bridges.

The substantial release of C3G at intestinal pH can be attributed to the absence of electrostatic attractions in acidic conditions. These findings underscore the importance of pH in modulating electrostatic interactions within nanostructured systems. Specifically, nanostructures designed under acidic conditions may offer a controlled release of C3G, potentially enhancing its absorption over prolonged periods. Moreover, our results shed light on the role of electrostatic forces in nanostructure behavior, offering insights into the design principles for optimizing bioactive compound delivery systems. In general, manipulating the charge characteristics of encapsulating materials can tailor release kinetics and enhance therapeutic efficacy. Therefore, the *in silico* findings corroborate our *in vivo* results and support our understanding of the controlled release observed in mice.

5. Conclusions and future perspectives

Many efforts have been made to promote better anthocyanin absorption, and several tools have been used in the last decades. The pectin and lysozyme-based nanoencapsulation used in our work proved effective in this objective. In summary, we developed a stable nanosystem using easy-to-implement technology. Environmentally safe compounds were added to nanoencapsulate anthocyanin based on pectin and lysozyme without potentially toxic compounds. The nanoformulation is effective for increasing absorption and reaching specific tissues. Nanoencapsulation can induce a delayed transit of anthocyanins from the stomach to the intestine and a longer maintenance time between absorption and excretion of the compound.

This study proposes a new methodology for the radioactive labeling of anthocyanins, which can be applied in molecular imaging and biodistribution studies. The method described can be transferred to a broader range of studies on nano-encapsulated polyphenolic compounds in various biological investigations, contributing to obtaining more effective results on bioavailability.

Notably, the anthocyanin within the nanostructure is prolonged in the body, possibly due to the protection provided by biomaterials and the nano-matrix effect. The anthocyanin may have been absorbed intact and delivered more efficiently to tissues than the free molecule. It can also be considered for the absorption of the intact nanoparticles. This represents an advance in studying the absorption of anthocyanins as a bioactive compound and an innovative strategy for high efficiency in biological use. Anthocyanins delivered into tissues are promising and have prospects for developing supplements to be used as adjuvants in treatments for some chronic non-communicable diseases, which could represent a substantial advance toward better human health.

In conclusion, we developed a stable and oriented nanostructure for delivery into different tissues. The technique used for the developed nanoformulation overcame a crucial limitation regarding stability and enabled the clinical future application of anthocyanin. Anthocyanin protection based on polysaccharide-protein structure can be used in targeted therapies, which should be further investigated. The *in vivo* approach used in this study demonstrated that the pectin and lysozyme-nanocapsule protect the anthocyanin and increase the absorption. A significant difference was observed between the absorption of free versus nanoencapsulated anthocyanins. The detected nanoencapsulated molecules in the blood after 24 h of ingestion indicate an alteration in the absorption kinetics, with extensive preservation of the bioactive compound within the organism, probably due to reduced degradation and improved absorption. The results revealed in this research prospect clinical applications and indicated the design of suitable anthocyanin-based nanoformulations for food, supplements, and pharmaceutical products.

The knowledge generated in this study is an essential tool in food science, mainly in the nanoencapsulation of plant bioactive compounds and their biological evaluation. The results also contribute to filling the gaps about anthocyanin bioavailability and instigating the development of precision therapies. Thus, nanoencapsulation constitutes a promising technology for promoting the bioavailability of anthocyanins and other polyphenolic compounds, providing a solid foundation for further research and development in intersectoral and interdisciplinary areas such as nutrition, pharmaceutical, and medicine.

Funding

The authors acknowledge The National Council for Scientific and Technological Development (CNPq) for the T.K.O.R. scholarship (#151150/2023-0) and J.P.F. productivity scholarship (#307842/2022-3). The authors acknowledge the São Paulo Research Foundation (FAPESP) for the T.K.O.R. scholarship (#2023/09620-3). The study was financially supported by grants #2013/07914-8, #2022/12834-2, and #2023/01396-7 from the São Paulo Research Foundation (FAPESP). Prof. H. A. Santos acknowledges financial support from the University Medical Center Groningen Research Funds.

CRediT authorship contribution statement

Thiécla Katiane Osvaldt Rosales: Writing – review & editing, Writing – original draft, Methodology, Investigation, Formal analysis, Data curation. **Fábio Fernando Alves da Silva:** Writing – review & editing, Methodology, Investigation, Formal analysis. **Andy Gonzàlez Rivera:** Writing – review & editing, Software, Formal analysis. **Sofia Nascimento dos Santos:** Writing – review & editing, Validation,

Methodology, Formal analysis. **Daniel Bustos:** Writing – review & editing, Software, Formal analysis. **Luis Alberto Morales-Quintana:** Writing – review & editing, Software, Formal analysis. **Hélder A. Santos:** Writing – review & editing, Validation. **Emerson Soares Bernardes:** Writing – review & editing, Validation, Supervision, Funding acquisition, Conceptualization. **João Paulo Fabi:** Writing – review & editing, Writing – original draft, Visualization, Validation, Supervision, Project administration, Funding acquisition, Conceptualization.

Declaration of competing interest

The authors declare that they have no known competing financial interests or personal relationships that could have appeared to influence the work reported in this paper.

Data availability

Data will be made available on request.

Acknowledgments

The authors acknowledge The National Council for Scientific and Technological Development (CNPq) for the T.K.O.R. scholarship (#151150/2023-0) and J.P.F. productivity scholarship (#307842/2022-3). The authors acknowledge the São Paulo Research Foundation (FAPESP) for the T.K.O.R. scholarship (#2023/09620-3). The study was financially supported by grants #2013/07914-8, #2022/12834-2, and #2023/01396-7 from the São Paulo Research Foundation (FAPESP). Prof. H. A. Santos acknowledges financial support from the University Medical Center Groningen Research Funds. The authors thank Dra. Iolanda Midea Cuccovia from the Chemistry Institute of São Paulo (IQ—USP) for the DLS equipment use.

Appendix A. Supplementary data

Supplementary data to this article can be found online at https://doi.org/10.1016/j.foodres.2024.115125.

References

Antonov, Y. A., Zhuravleva, I. L., Celus, M., Kyomugasho, C., Hendrickx, M., Moldenaers, P., & Cardinaels, R. (2021). Effect of overall charge and local charge density of pectin on lysozyme's structure and thermal stability. *Journal of Thermal Analysis and Calorimetry, 16*, 3133–3314. https://doi.org/10.1007/s10973-021-10954-5

Ayvaz, H., Cabaroglu, T., Akyildiz, A., Pala, C. U., Temizkan, R., Ağçam, E., Ayvaz, Z., Durazzo, A., Lucarini, M., Direito, R., & Diaconeasa, Z. (2023). Anthocyanins : Metabolic Digestion, Bioavailability, Therapeutic Effects, Current Pharmaceutical/Industrial Use, and Innovation Potential. *Antioxidants, 12*, 48. https://doi.org/10.3390/antiox12010048

Bondonno, N. P., Dalgaard, F., Kyro, C., Murray, K., Bondonno, C. P., Lewis, J. R., Croft, K. D., Gislason, G., Scalbert, A., Cassidy, A., Tjonneland, A., Overvad, K., & Hodgson, J. M. (2019). Flavonoid intake is associated with lower mortality in the Danish Diet Cancer and Health Cohort. *Nature Communications, 10*, 3651. https://doi.org/10.1038/s41467-019-11622-x

Braga, A. R. C., Murador, D. C., de Souza Mesquita, L. M., & de Rosso, V. V. (2018). Bioavailability of anthocyanins: Gaps in knowledge, challenges, and future research. *Journal Food Composition and Analysis, 68*, 31–40. https://doi.org/10.1016/j.jfca.2017.07.031

Brodkorb, A., Egger, L., Alminger, M., et al. (2019). INFOGEST static *in vitro* simulation of gastrointestinal food digestion. *Nature Protocols, 14*, 991–1014. https://doi.org/10.1038/s41596-018-0119-1

Bustos, D., Guzmán, L., Valdés, O., Muñoz-Vera, M., Morales-Quintana, L., & Castro, R. I. (2023). Development and Evaluation of Cross-Linked Alginate – Chitosan – Abscisic Acid Blend Gel. *Polymers, 28*, 3217. https://doi.org/10.3390/polym15153217

Chatterjee, N. S., Dara, P. L., Sreerekha, P. R., Vijayan, D. K., Sadasivam, J., Mathew, S., Ravishankar, C. N., & Anandan, R. (2021). Nanoencapsulation in low-molecular-weight chitosan improves the in vivo antioxidant potential of black carrot anthocyanin. *Journal Science Food and Agriculture, 101*, 5264–5271. https://doi.org/10.1002/jsfa.11175

Chen, Y., Chen, H., Zhang, W., Ding, Y., Zhao, T., Zhang, M., Mao, G., Feng, W., & Wu, X. L. Y. (2020). Bioaccessibility and biotransformation of anthocyanin monomers following in vitro simulated gastric-intestinal digestion and in vivo metabolism in rats. *Food Function, 10*, 6052–6061. https://doi.org/10.1039/d0fo90028a

Chen, Y., Zhao, L., Qian, W., & Zhou, B. (2023). Pharmacokinetics of cyanidin-3- *O* -galactoside and cyanidin-3- *O* -arabinoside after intravenous administration in rats. *CurrentCurrent Issues Molecular Biology, 26*, 2884–2925. https://doi.org/10.3390/cimb46040181

Custodio-Mendoza, J. A., Aktaş, H., Zalewska, M., Wyrwisz, J., & Kurek, M. A. (2024). A Review of Quantitative and Topical Analysis of Anthocyanins in Food. *Molecules, 29*(8), 1735. https://doi.org/10.3390/molecules29081735

Czank, C., Cassidy, A., Zhang, Q., Morrison, D. J., Preston, T., Kroon, P. A., Botting, N. P., & Kay, C. D. (2013). Human metabolism and elimination of the anthocyanin, cyanidin-3-glucoside : A ^{13}C-tracer study. *The American Journal of Clinical Nutrition, 97*, 995–1003. https://doi.org/10.3945/ajcn.112.049247

Fang, J., Luo, Y., Yuan, K., Guo, Y., & Jin, S. (2020). Preparation and evaluation of an encapsulated anthocyanin complex for enhancing the stability of anthocyanin. *LWT - Food Science Technology, 117*, Article 108543. https://doi.org/10.1016/j.lwt.2019.108543

Felgines, C., Krisa, S., Mauray, A., Besson, C., Lamaison, J., Scalbert, A., … Texier, O. (2010). Radiolabelled cyanidin 3- O -glucoside is poorly absorbed in the mouse. *British Journal of Nutrition, 103*, 1738–1745. https://doi.org/10.1017/S0007114510000061

Giusti, M., & Wrolstad, R. E. (2005). Characterization and Measurement of Anthocyanins by UV-visible Spectroscopy. *Current Protocols in Food Analytical Chemistry, 2*, 19–31. https://doi.org/10.1002/0471142913.faf0102s00

Hahm, T. H., Tanaka, M., & Matsui, T. (2022). Current Knowledge on Intestinal Absorption of Anthocyanins. *Journal Agricultural Food Chemistry, 70*, 2501–2509. https://doi.org/10.1021/acs.jafc.1c08207

He, Y., Chen, D., Liu, Y., Sun, X., Guo, W., An, L., Shi, Z., Wen, L., Wang, Z., & Yu, H. (2022). Protective Effect and Mechanism of Soybean Insoluble Dietary Fiber on the Color Stability of Malvidin-3- O -glucoside. *Foods, 11*, 1474. https://doi.org/10.3390/foods11101474

Hee, M., Rho, J. K., Kang, J. A., Shim, H. E., Nam, Y. R., Yoon, S., Kim, H. R., Choi, D. S., Park, S. H., Jang, B. J., & Jeon, J. (2016). Efficient radiolabeling of rutin with 125 I and biodistribution study of radiolabeled rutin. *Journal of Radioanalytical and Nuclear Chemistry, 308*, 477–483. https://doi.org/10.1007/s10967-015-4415-8

Hou, Y., Wei, W., Guan, X., Liu, Y., Bian, G., He, D., Fan, Q., Cai, X., Zhang, Y., Wang, G., Zheng, X., & Hao, H. (2021). A diet-microbial metabolism feedforward loop modulates intestinal stem cell renewal in the stressed gut. *Nature Communications, 12*, 271. https://doi.org/10.1038/s41467-020-20673-4

Igwe, E. O., Charlton, K. E., Probst, Y. C., Kent, K., & Netzel, M. E. (2019). A systematic literature review of the effect of anthocyanins on gut microbiota populations. *Journal of Human Nutrition Dietetics, 32*, 53–62. https://doi.org/10.1111/jhn.12582

Jaime, L., & Santoyo, S. (2021). The health benefits of the bioactive compounds in foods. *Foods, 10*, 3–6. https://doi.org/10.3390/foods10020325

Kalt, W. (2019). Anthocyanins and Their C6–C3 - C6 Metabolites in Humans and Animals. *Molecules, 24*, 4024. https://doi.org/10.3390/molecules24224024

Kapoor, P., Tiwari, A., Sharma, S., Tiwari, V., Sheoran, B., Ali, U., & Garg, M. (2023). Effect of anthocyanins on gut health markers, Firmicutes - Bacteroidetes ratio and short-chain fatty acids : A systematic review via meta-analysis. *Scientific Reports, 31*, 1–16. https://doi.org/10.1038/s41598-023-28764-0

Li, L., Li, J., Xu, H., Zhu, F., Li, Z., Lu, H., Zhang, J., Yang, Z., & Liu, Y. (2021). The Protective Effect of Anthocyanins Extracted from Aronia Melanocarpa Berry in Renal Ischemia-Reperfusion Injury in Mice. *Mediators of Inflammation, 22*, 7372893. https://doi.org/10.1155/2021/7372893

Marques, C., Fernandes, I., Meireles, M., & Faria, A. (2018). Gut microbiota modulation accounts for the neuroprotective properties of anthocyanins. *Scientific Reports, 8*, 11341. https://doi.org/10.1038/s41598-018-29744-5

Manolescu, B. N., Oprea, E., Mititelu, M., Ruta, L. L., & Farcasanu, I.-C. (2019). Dietary Anthocyanins and Stroke: A Review of Pharmacokinetic and Pharmacodynamic Studies. *Nutrients, 11*, 1479. https://doi.org/10.3390/nu11071479

Martínez, L., Andrade, R., Birgin, E. G., & Martínez, J. M. (2009). PACKMOL: A package for building initial configurations for molecular dynamics simulations. *Journal Computacional Chemistry, 30*, 2157–2164. https://doi.org/10.1002/jcc.21224

Millar, C. L., Duclos, Q., & Blesso, C. N. (2017). Effects of Dietary Flavonoids on Reverse Cholesterol Transport, HDL Metabolism. *Advances in Nutrition, 8*, 226–239. https://doi.org/10.3945/an.116.014050

Mozos, I., Flangea, C., Vlad, D. C., Gug, C., Mozos, C., Stoian, D., Luca, C. T., Horbańczuk, J. O., Horbańczuk, O. K., & Atanasov, A. G. (2021). Effects of Anthocyanins on Vascular Health. *Biomolecules, 11*, 1–22. https://doi.org/10.3390/biom11060811

Oliveira, H., Roma-Rodrigues, C., Santos, A., Veigas, B., Brás, N., Faria, A., Calhau, C., de Freitas, V., Baptista, P. V., Mateus, N., Fernandes, A. R., & Fernandes, I. (2019). GLUT1 and GLUT3 involvement in anthocyanin gastric transport- Nanobased targeted approach. *Scientific Reports, 9*, 789. https://doi.org/10.1038/s41598-018-37283-2

Osvaldt Rosales, T. K., Pessoa da Silva, M., Lourenço, F. R., Aymoto Hassimotto, N. M., Fabi, J. P. (2021). Nanoencapsulation of anthocyanins from blackberry (*Rubus* spp.) through pectin and lysozyme self-assembling. *Food Hydrocolloids*, 114, 106563. https://doi.org/10.1016/j.foodhyd.2020.106563.

Pieczywek, P. M., Płaziński, W., & Zdunek, A. (2020). Dissipative particle dynamics model of homogalacturonan based on molecular dynamics simulations. *Scientific Reports, 10*, 14691. https://doi.org/10.1038/s41598-020-71820-2

Qi, Q., Chu, M., Yu, X., Xie, Y., Li, Y., Du, Y., & Yan, N. (2022). Anthocyanins and Proanthocyanidins: Chemical Structures, Food Sources, Bioactivities, and Product Development. *Food Reviews International, 39*(7), 4581–4609. https://doi.org/10.1080/87559129.2022.2029479

Quek, Y. Y., Cheng, L. J., Ng, Y. X., Hey, H. W. D., & Wu, X. V. (2023). Effectiveness of anthocyanin-rich foods on bone remodeling biomarkers of middle-aged and older adults at risk of osteoporosis: A systematic review, meta-analysis, and meta-regression. *Nutrition Review, 121*, 1923–1940. https://doi.org/10.1093/nutrit/nuad121

Roos, K., Wu, C., Damm, W., Reboul, M., Stevenson, J. M., Lu, C., Dahlgren, M. K., Mondal, S., Chen, W., Wang, L., Abel, R., Friesner, R.,A., Harder, E. D. (2019). OPLS3e: Extending Force Field Coverage for Drug-Like Small Molecules. *Journal of Chemical Theory and Computation*, 15, 1863-1874. https://doi.org/10.1021/acs.jctc.8b01026.

Rosales, T. K. O., & Fabi, J. P. (2023). Polysaccharide-based nanotechnology approaches to deliver bioactive compounds for food applications [Internet]. *Advances in Chemical Engineering, 62*, 215–256. https://doi.org/10.1016/bs.ache.2023.08.001

Rosales, T. K. O., & Fabi, J. P. (2022). Colloids and Surfaces B : Biointerfaces Nanoencapsulated anthocyanin as a functional ingredient : Technological application and future perspectives. *Colloids Surface B Biointerface, 218*, Article 112707. https://doi.org/10.1016/j.colsurfb.2022.112707

Rosales, T. K. O., Hassimotto, M. N., Lajolo, F. M., & Fabi, J. P. (2022). Nanotechnology as a Tool to Mitigate the Effects of Intestinal Microbiota on Metabolization of Anthocyanins. *Antioxidants., 11*, 506. https://doi.org/10.3390/antiox11030506

Rosales, T. K. O., Pedrosa, L. F., Fioroto, A. M., Toniazzo, T., Tadini, C. C., Purgato, E., … Fabi, J. P. (2023b). Nanoencapsulated anthocyanins : A new technological approach to increase physical-chemical stability and bioaccessibility. *Food Hydrocolloids, 139*, Article 108516. https://doi.org/10.1016/j.foodhyd.2023.108516

Rosales, T. K. O., Silva, F. F. A., Bernardes, E. S., & Fabi, J. P. (2023a). Plant-derived polyphenolic compounds : Nanodelivery through polysaccharide-based systems to improve the biological properties. *Critical Review Food Science Nutrition, 10*, 1–25. https://doi.org/10.1080/10408398.2023.2245038

Salah, M., Mansour, M., Zogona, D., & Xu, X. (2020). Nanoencapsulation of anthocyanins-loaded β-lactoglobulin nanoparticles: Characterization, stability, and bioavailability *in vitro*. *Food Research Internacional, 137*, Article 109635. https://doi.org/10.1016/j.foodres.2020.109635

Salarbashi, D., Bazeli, J., Rad, E. F. (2020). An update on the new achievements in the nanocapsulation of anthocyanins. *Nanomedicine Journal*, 7, 87–97. https://doi.org/10.22038/nmj.2020.07.001.

Salhotra, A., Shah, H. N., Levi, B., & Longaker, M. T. (2020). Mechanisms of bone development and repair. *Nature Reviews Molecular Cell Biology, 21*, 696–711. https://doi.org/10.1038/s41580-020-00279-w

Sandoval-Ramírez, B. A., Catalán, Ú., Fernández-Castillejo, S., Rubió, L., Macià, A., & Solà, R. (2018). Anthocyanin Tissue Bioavailability in Animals: Possible Implications for Human Health. A Systematic Review. *Journal Agricultural Food Chemistry, 66*, 11531–11543. https://doi.org/10.1021/acs.jafc.8b04014

Schrödinger, L. L. C. (2021). Schrödinger Release. LigPrep. 3 (Schrödinger, LLC, New York, NY, 2021).

Shelley, J. C., Cholleti, A., Frye, L. L., Greenwood, J. R., Timlin, M. R., & Uchimaya, M. (2007). Epik: A software program for pKa prediction and protonation state generation for drug-like molecules. *Journal of Computer-Aided Molecular Design, 21*, 681–691. https://doi.org/10.1007/s10822-007-9133-z

Silva, M. P., Rosales, T. K. O., Pedrosa, L. F., & Fabi, J. P. (2022). Formulation of a New Proof-of-concept Pectin/lysozyme Nanocomplex as Potential β- lactose Delivery Matrix: Structure and Thermal Stability Analyses. *Food Hydrocolloids, 134*, Article 108011. https://doi.org/10.1016/j.foodhyd.2022.108011

Tarone, A. G., Cazarin, C. B. B., & Marostica Junior, M. R. (2020). Anthocyanins: New techniques and challenges in microencapsulation. *Food Research Internacional, 133*, Article 109092. https://doi.org/10.1016/j.foodres.2020.109092

Teixeira, L. D. L., Bertoldi, F. C., Lajolo, F. M., & Hassimotto, N. M. A. (2015). Identification of Ellagitannins and Flavonoids from Eugenia brasilienses Lam. (Grumixama) by HPLC-ESI-MS/MS. *Journal Agricultural Food Chemistry, 63*, 5417–5427. https://doi.org/10.1021/acs.jafc.5b01195

Tena, N., Martín, J., & Asuero, A. G. (2020). State of the art of anthocyanins: Antioxidant activity, sources, bioavailability, and therapeutic effect in human health. *Antioxidants, 9*, 451. https://doi.org/10.3390/antiox9050451

Valdes, O., Bustos, D., Guzmán, L., Muñoz-Vera, M., Urra, G., Castro, R. I., & Morales-Quintana, L. (2024). The Controlled Release of Abscisic Acid (ABA) Utilizing Alginate – Chitosan Gel Blends : A Synergistic Approach for an Enhanced Small-Molecule Delivery Controller. *Gels, 10*, 185. https://doi.org/10.3390/gels10030185

Van de Velde, F., Pirovani, M. E., & Drago, S. R. (2018). Bioaccessibility analysis of anthocyanins and ellagitannins from blackberry at simulated gastrointestinal and colonic levels. *Journal of Food Composition and Analysis, 72*, 22–31. https://doi.org/10.1016/j.jfca.2018.05.007

Verediano, T. A., Martino, H. S. D., Dias Paes, M. C., & Tako, E. (2021). Effects of anthocyanin on intestinal health: A systematic review. *Nutrients, 13*, 1331. https://doi.org/10.3390/nu13041331

Victoria-Campos, C. I., Ornelas-Paz, J. J., Rocha-Guzmán, N. E., Gallegos-Infante, J. A., Failla, M. L., Pérez-Martínez, J. D., Rios-Velasco, C., & Ibarra-Junquera, V. (2022). Gastrointestinal metabolism and bioaccessibility of selected anthocyanins isolated from commonly consumed fruits. *Food Chemistry., 383*. https://doi.org/10.1016/j.foodchem.2022.132451

Xue, H., Sang, Y., Gao, Y., Zeng, Y., & Liao, J. (2023). Research Progress on Absorption, Metabolism, and Biological Activities of Anthocyanins in Berries : A Review. *Antioxidants, 20*, 1–22. https://doi.org/10.3390/antiox12010003

You, W.; Zheng, W.; Weiss, S.; Chua, K. F.; Steegborn, C. Structural basis for activating and inhibiting Sirtuin 6 by quercetin and its derivatives (2019). *Scientific Reports*, 9, 19176. https://doi.org/10.1038/s41598-019-55654-1.

Zhang, A., Meng, K., Liu, Y., Pan, Y., Qu, W., Chen, D., & Xie, S. (2020). Absorption, distribution, metabolism, and excretion of nanocarriers *in vivo* and their influences. *Advances in Colloid and Interface Science, 284*, Article 102261. https://doi.org/10.1016/j.cis.2020.102261

Zhao, X., Tie, S., Hou, S., Wang, H., Song, Y., Rai, R., & Tan, M. (2020). Facile synthesis of nano-nanocarriers from chitosan and pectin with improved stability and biocompatibility for anthocyanins delivery: An *in vitro* and *in vivo* study. *Food Hydrocolloids, 109*, Article 106114. https://doi.org/10.1016/j.foodhyd.2020.106114

Zhong, H., Xu, J., Yang, M., Hussain, M., Liu, X., Feng, F., & Guan, R. (2023). Protective Effect of Anthocyanins against Neurodegenerative Diseases through the Microbial-Intestinal-Brain Axis. *Nutrients, 15*, 496. https://doi.org/10.3390/nu15030496